JOURNAL OF Applied Polymer SCIENCE

Effect of Surface Acetylated-Chitin Nanocrystals on Structure and Mechanical Properties of Poly(lactic acid)

Qiaoxin Zhang,[1] Siwen Wei,[1] Jin Huang,[2,3] Jiwen Feng,[4] Peter R. Chang[5]

[1]School of Materials Science and Engineering, Wuhan University of Technology, Wuhan 430070, China
[2]College of Chemical Engineering, Wuhan University of Technology, Wuhan 430070, China
[3]State Key Laboratory of Pulp and Paper Engineering, South China University of Technology, Guangzhou 510640, China
[4]State Key Laboratory of Magnetic Resonance and Atomic and Molecular Physics, Wuhan Institute of Physics and Mathematics, Chinese Academy of Sciences, Wuhan 430071, China
[5]BioProducts and Bioprocesses National Science Program, Agriculture and Agri-Food Canada, Saskatoon, SK, S7N 0X2, Canada
Correspondence to: J. Huang (E-mail: huangjin@iccas.ac.cn) or P. R. Chang (E-mail: peter.chang@agr.gc.ca)

ABSTRACT: In this work, the miscibility between chitin nanocrystals (ChNs) and poly(lactic acid) (PLA) was expected to be improved by surface acetylation of ChN. The reaction of acetic anhydride onto the ChN surface was confirmed by FTIR and ^{13}C NMR, while XRD and TEM proved the crystalline structure and rod-like morphology were maintained. The acetylated ChN (AChN) was incorporated into a PLA matrix by solution blending, and resulted in an increase of tensile strength and Young's modulus and they reached to the maximum value as 45 and 37% higher than neat PLA film, respectively, with the loading level of AChN reaching to 4 wt %. The enhancement could be attributed to that acetylation improved dispersion of AChN in the PLA matrix and interfacial adhesion between AChN and PLA. The performances of the nanocomposites based on PLA and chitin nanocrystals derived from renewable resources have good potential for industrial applications. © 2013 Wiley Periodicals, Inc. J. Appl. Polym. Sci. **2014**, *131*, 39809.

KEYWORDS: biodegradable; composites; mechanical properties; polysaccharides; chitin nanocrystal; poly(lactic acid)

Received 28 May 2013; accepted 1 August 2013
DOI: 10.1002/app.39809

INTRODUCTION

Because of increasing concern about the environment, the development of biodegradable plastics for application in different fields has aroused great interest.[1] Poly(lactic acid) (PLA) results from the polymerization of lactic acid, which is derived from renewable resources such as corn or potato starch, thus making it a very attractive material.[2] PLA has good mechanical properties and processability similar to petroleum-based plastics, and thus it has a great potential to replace them.[3–5] Containers, drinking cups, salad cups, over wrap and lamination films, and blister packages are currently being made from PLA,[6–8] and its application could broaden if the problems of high production cost, intrinsic brittleness and thermal stability can be resolved.[9–11] Therein, blending PLA with other polymers provides a good resolution. Polysaccharide nanocrystals have aroused a great deal of interest for their nanoscale dimensions, high surface area, low density, nontoxicity and high mechanical strength, as well as the fact that they are readily available, renewable, biocompatible, highly reactive, easily processed and biodegradable.[12–14] There have been several reports of studies aimed at enhancing toughness and strain at break of PLA with polysaccharide nanocrystals such as cellulose[15–19] and starch.[20–24]

Although polysaccharide nanocrystals are promising fillers, there are some drawbacks that need to be overcome. Polysaccharide nanocrystals have a high surface area and a hydrophilic nature, with intermolecular and intramolecular hydrogen bonding that easily emerge resulting in aggregation of the nanocrystals; thus compounding with most nonpolar thermoplastics is inefficient.[25–27] Therein, the surface properties of nanocrystals need to be modified to inhibit self-aggregation and improve dispersion and interfacial adhesion in various polymeric matrices. Besides, during modification the original crystalline structure of the nanocrystals should not be destroyed. Surface acetylation of polysaccharide nanocrystals has been proved to be an effective method of modification. There have been many studies on acetylation of polysaccharide nanocrystals to overcome poor dispersion in hydrophobic polymer matrices and enhance interfacial bonding, thereby improving mechanical properties of the nanocomposites.[28–30]

Chitin is similar to cellulose in structure except there are acetamide groups at the C-2 positions of chitin in place of the hydroxyl groups of cellulose.[31,32] Chitin nanocrystals easily self-aggregate and can form micrometer scale agglomerates in a hydrophobic polymer matrix. Also, due to the many hydroxyl

groups on the surface of chitin nanocrystals, they are hydrophilic. Because the hydroxyl groups are very reactive, they are easy to modify using various surface chemical reactions to improve the hydrophobicity of chitin nanocrystals.[33] In this work, chitin nanocrystals were acetylated and then incorporated into a PLA matrix, and hence was expected to contribute to the higher rigidity of the resultant nanocomposites.

MATERIALS AND METHODS

Materials

Commercial poly(lactic acid) (PLA) pellets were purchased from Shenzhen BrightChina Industrial (Shenzhen, China). The number-average molar weight and polydispersity of PLA were 8.1×10^4 Da and 1.80, respectively, and the content of L-lactic acid was about 99%. Chitin (crab shell) was purchased from Yuhuan Ocean Biochemical (Zhejiang, China). Acetic anhydride was purchased from Xilong Chemical Industry (Shantou, China). Pyridine was dried and purified according to standard procedures. Hydrochloric acid (HCl), dichloromethane (CH_2Cl_2), acetone (C_3H_6O) and other analytical grade reagents were purchased from Shanghai Sinopharm Chemical Reagent (Shanghai, China) and used without further purification.

Extraction of Chitin Nanocrystals

Chitin nanocrystals (ChNs) were prepared according to the previous report by Nair and Dufresne[34]: Crab chitin was boiled and mechanically stirred in a 5% KOH solution for 6 h to remove most of the proteins. It was then stirred at room temperature overnight, filtered, and washed with distilled water. The resultant solid was bleached with 17 g of $NaClO_2$ in 1 L of water containing 0.3 *M* CH_3COONa buffer for 6 h at 80°C; the bleach solution was changed every 2 h. After that, the suspension was kept in a 5% KOH solution for 48 h to remove residual proteins and then centrifuged at 3600 rpm for 15 min. The resultant chitin was hydrolyzed with boiling 3 *N* HCl for 90 min under mechanical stirring (the ratio of 3 *N* HCl to chitin was 30 mL HCl per 1 g chitin). Finally, the acid hydrolyzed suspension was diluted with distilled water and centrifuged (3600 rpm for 15 min). This was repeated three times before dialyzing until the pH reached 4.0. The suspension was then dialyzed overnight against distilled water and finally, the loose chitin nanocrystal powder was obtained after freeze-drying.

Acetylation of Chitin Nanocrystals

One gram of ChN was dispersed in 20 mL anhydrous pyridine, and then added to a flask after ultrasonic treatment for 15 min. About 5 mL acetic anhydride was added to anhydrous pyridine, which was then added dropwise to the ChN suspension. The reaction mixture was kept at 80°C and stirred at 400 rpm for 5 h. After that, the product was isolated by precipitation in 1.0 L water and washed three times. It was then purified by washing with a solution of acetone/water to eliminate all non-bonded chemicals. Finally, the acetylated chitin whisker powder, coded as AChN, was obtained after freeze-drying.

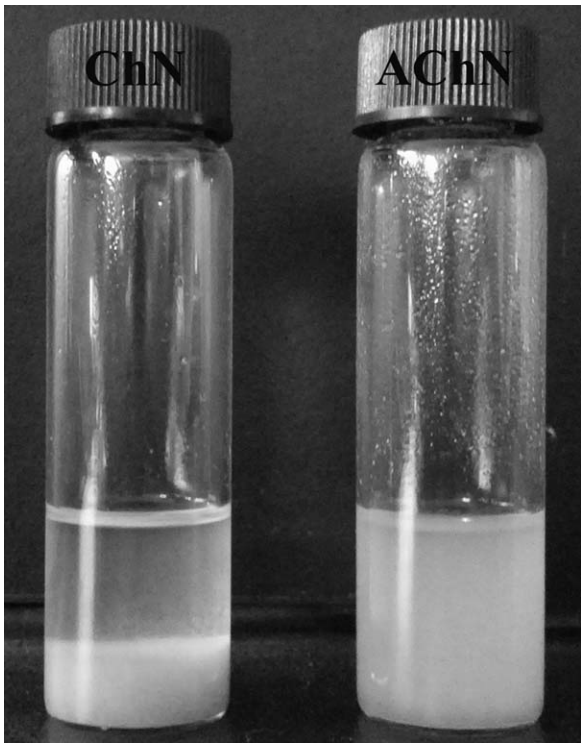

Figure 1. Dispersibility of the ChN and AChN in dichloromethane.

Preparation of PLA Nanocomposites Filled with AChN

The surface acetylated chitin nanocrystals showed improved dispersion in CH_2Cl_2, as seen in Figure 1. A certain amount of AChN and 2.0 g PLA were added to CH_2Cl_2, and then stirred to produce a mixture which was conditioned overnight to eliminate bubbles before being cast into a Teflon mould. The CH_2Cl_2 evaporated off when kept at ambient temperature for 24 h. The films solidified and were kept in a desiccator containing silica gel. The amount of AChN added were 0, 1, 2, 4, 6, 8, and 10 wt % and the resultant nanocomposite films were coded as

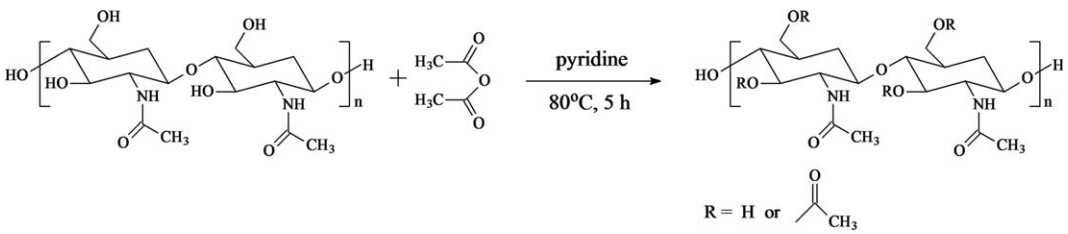

Figure 2. Surface acetylation of chitin nanocrystals by the reaction between hydroxyl groups of chitin nanocrystals and acetic anhydride.

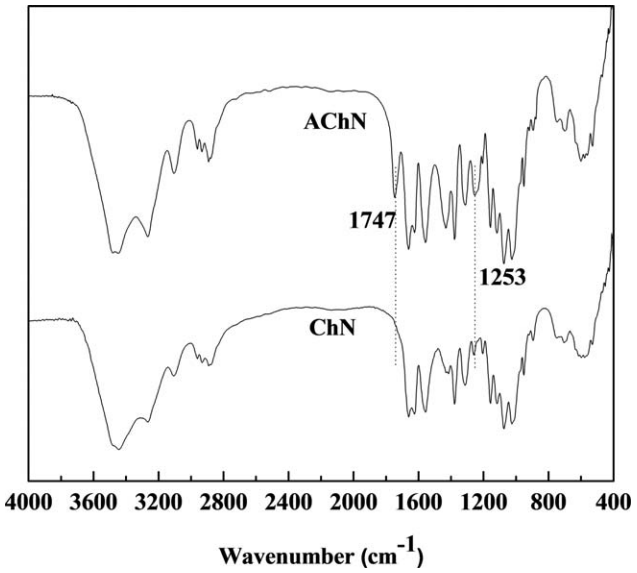

Figure 3. FT-IR spectra of the ChN and AChN powders.

PLA, PLA/AChN-1, PLA/AChN-2, PLA/AChN-4, PLA/AChN-6, PLA/AChN-8, and PLA/AChN-10.

CHARACTERIZATION

Fourier Transform Infrared (FT-IR) Spectroscopy

FTIR spectra of the powdered ChN and AChN were recorded on a 5700 FTIR spectrometer (Thermo Fisher, Madison, WI) and were scanned using a KBr-pellet method in the range of 4000–400 cm^{-1}.

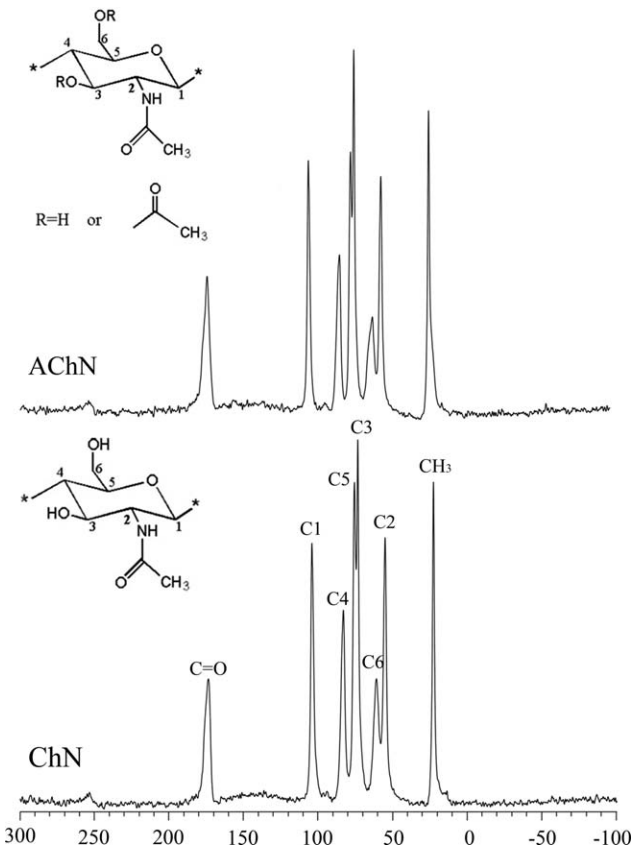

Figure 4. ^{13}C CP-MAS NMR spectra of the ChN and AChN powders.

Table I. Chemical Shifts and Areas of the Peaks and Their Assignments in the ^{13}C NMR Spectra of ChN and AChN

Chemical shift (ppm)	Assignment	Peak area	
		ChN	AChN
174.8	C=O	551.0	763.6
103.4	C1	675.5	675.5
83.1	C4	626.7	565.7
76.2,74.1	C5, C3	1450.2	1349.7
60.5	C6	526.6	500.3
56.3	C2	740.4	682.9
22.2	CH_3	623.9	762.7

X-ray Diffraction Analysis (XRD)

X-ray diffraction measurements were performed on dry powders of ChN and AChN, as well as on all nanocomposite sheets, at ambient temperature on a D/Max-IIIA X-ray diffractometer (Rigaku Denki, Tokyo, Japan) using Cu Kα radiation (λ = 0.154 nm) at 40 kV and 60 mA. The diffraction angle of 2θ ranged from 5 to 50°.

^{13}C CP-MAS NMR Spectroscopy

Solid state ^{13}C cross polarization-magic angle spinning (CP-MAS) NMR spectra of ChN and AChN were recorded at ambient temperature on a Varian Infinity-Plus 300 NMR spectrometer, using a MAS rate of 6 kHz, at a frequency of 75.5 MHz for ^{13}C NMR. Samples were packed in 4-mm-diameter zirconia MAS rotors. All spectra were run for 3 h (3000 scans).

Transmission Electron Microscopy (TEM)

TEM observations were carried out on an H-7000FA electron microscope (Hitachi, Tokyo, Japan) at 75 kV. Small amounts of powdered ChN and AChN were dispersed separately in distilled water, and then negatively stained with a 2% (w/v) uranyl acetate in ethanol solution.

Tensile Measurements

The tensile strength (σ_b), elongation at break (ε_b) and Young's modulus (E) were measured on a CMT6503 universal testing machine (SANS, Shenzhen, China) with a crosshead rate of 10 mm min^{-1} according to method ISO 527-3:1995(E). The tested specimens were cut into quadrate strips with the width of 10 mm, and the distance between testing marks was 30 mm. The average value of at least five replicates of each sample was taken.

Scanning Electron Microscope (SEM)

SEM observations were carried out on a X-650 scanning electron microscope (Hitachi, Tokyo, Japan) with an accelerating voltage of 25 kV. All nanocomposite films were frozen in liquid nitrogen and then immediately snapped. The fracture surfaces of the sheets were sputtered with gold and then observed and photographed.

Differential Scanning Calorimetry (DSC)

The DSC experiments were performed on a DSC instrument (Diamond DSC, PerkinElmer, MA) under a nitrogen

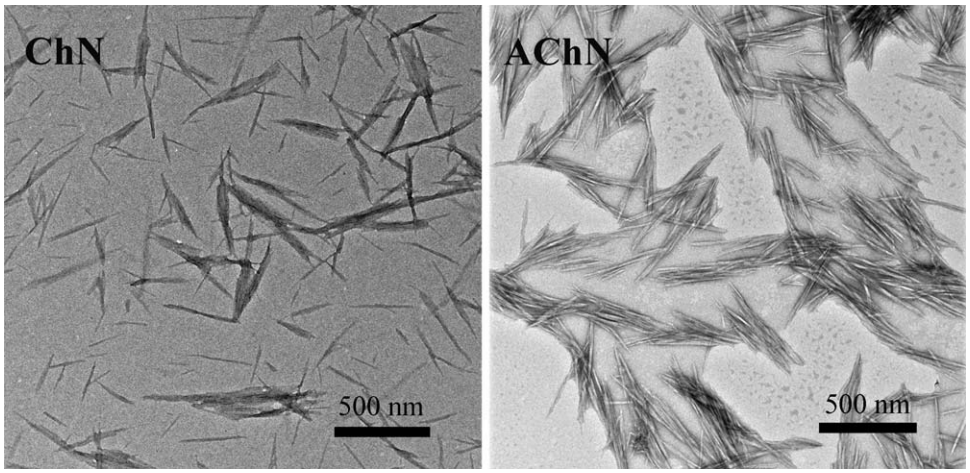

Figure 5. TEM images of the ChN and AChN powders.

atmosphere at a heating or cooling rate of 20°C min^{-1}. All nanocomposite films were scanned over a range of −50 to 200°C after a pretreatment of heating from 20 to 100°C and then cooling to −50°C to remove the residual solvent or other volatile.

RESULTS AND DISCUSSION

Structure of Acetylated Chitin Nanocrystals

The expected chemical reaction scheme of the acetylation of chitin nanocrystals is shown in Figure 2. The FT-IR spectra of chitin nanocrystals and acetylated chitin nanocrystals, shown in Figure 3, demonstrated that surface acetylation of chitin nanocrystals occurred. Compared to unmodified ChN, in AChN a new band appeared at 1747 cm^{-1} which corresponded to C═O stretching vibration modes of the acetyl group, and a band at 1253 cm^{-1}, which corresponded to C—O stretching vibration modes of the acetyl group, increased after the chemical reaction. ^{13}C CP-MAS NMR spectroscopy was also used to confirm surface acetylation of ChN. As we can see in the chemical reaction scheme in Figure 2, after the reaction some of the hydroxyl groups of ChN had been replaced by acetyl groups, thus the size of peaks corresponding to C═O and CH_3 of AChN were both larger after acetylation. As we can see in Figure 4 and Table I, this result was also consistent with the FT-IR results.

The morphological changes of ChN after acetylation were investigated by TEM. Before acetylation ChN, with lengths ranging from 114 to 320 nm and widths from 8 to 17 nm, had a spindle shape which was retained after surface modification by acetic anhydride (as shown in the TEM images in

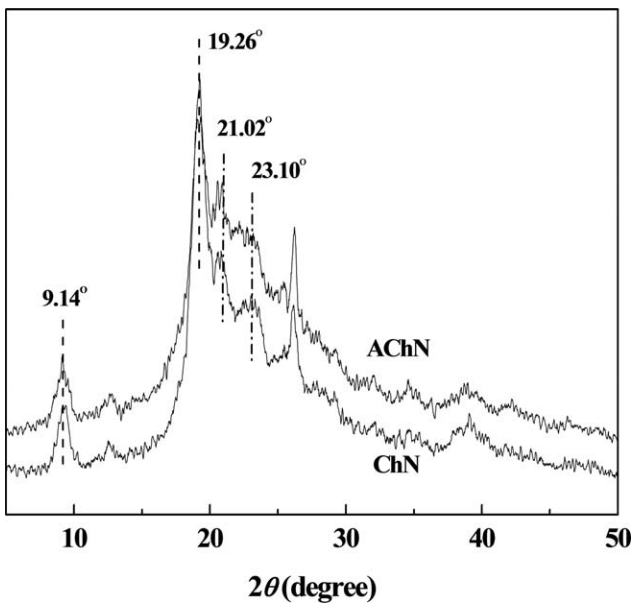

Figure 6. XRD patterns of the ChN and AChN powders.

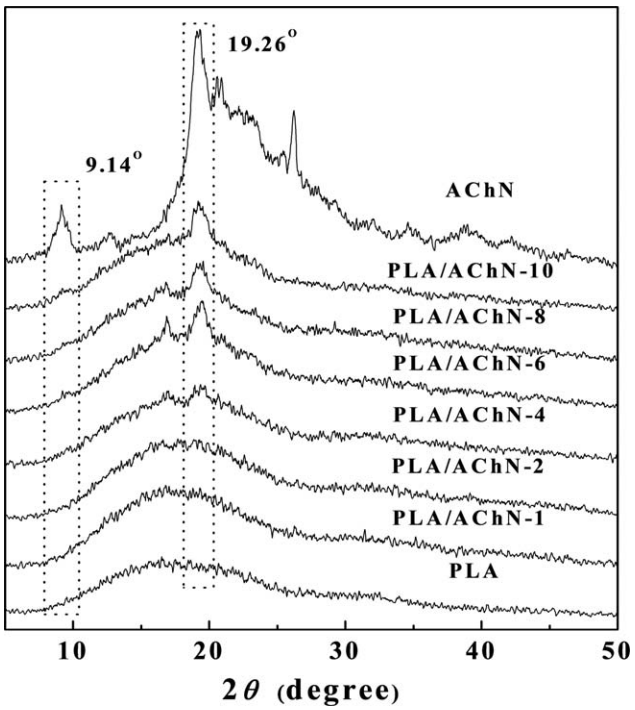

Figure 7. XRD patterns of the PLA/AChN nanocomposite films containing various loading levels of AChN as well as the neat PLA film and the AChN powder.

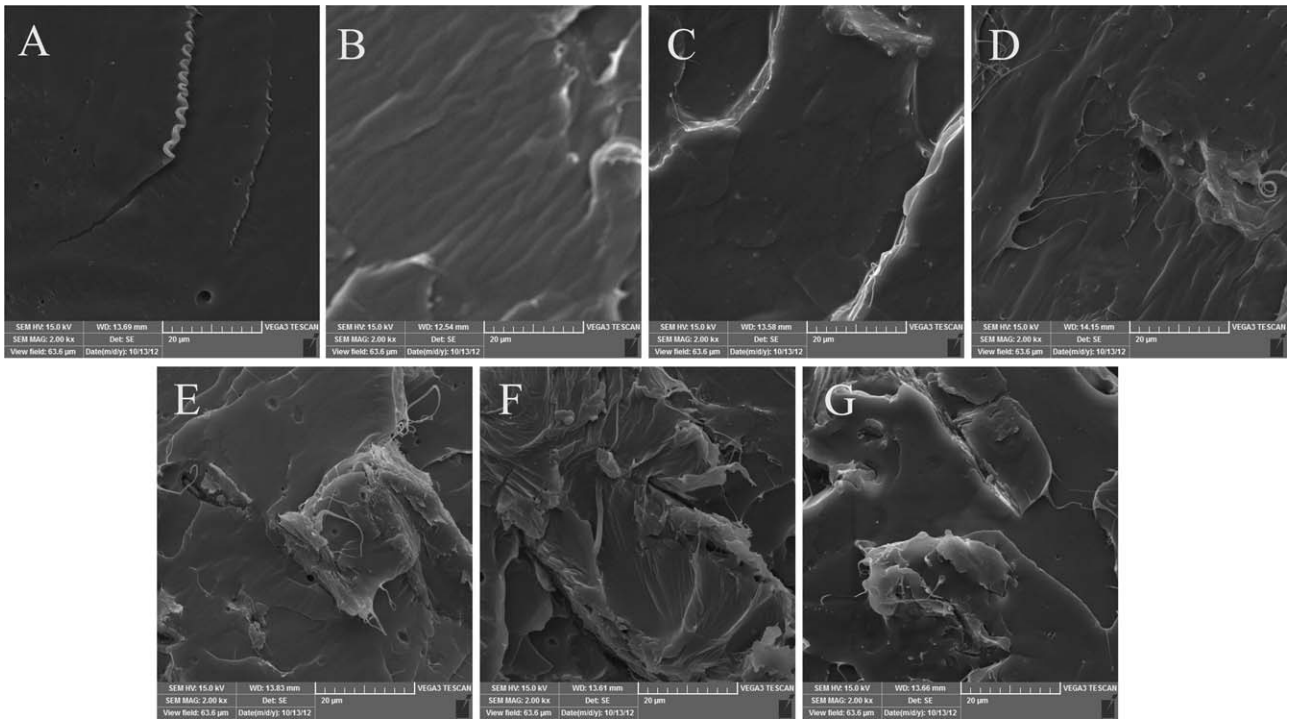

Figure 8. SEM images of the fractured surfaces of the nanocomposites of PLA/AChN-1 (B), PLA/AChN-2 (C), PLA/AChN-4 (D), PLA/AChN-6 (E), PLA/AChN-8 (F), PLA/AChN-10 (G) as well as the neat PLA film (A).

Figure 5). The X-ray diffraction profiles of ChN and AChN are shown in Figure 6. The four diffraction peaks of chitin nanocrystals observed at 9.14°, 19.26°, 21.02°, 23.10°, 26.5°, corresponding to 020, 110, 120, 130, 013 planes, respectively, show the typical antiparallel crystal pattern of α-chitin.[35–40] The crystalline intensities of AChN were similar to ChN, indicating that the inner crystalline structure of ChN was preserved after modification, which is consistent with the TEM results.

Crystalline Structure of PLA/AChN Nanocomposites

XRD patterns for PLA/AChN nanocomposites, as well as AChN, are shown in Figure 7. The PLA/AChN nanocomposites with low loading levels of 1 and 2 wt % AChN showed diffraction patterns similar to that of the neat PLA film, which may be attributed to the homogeneous dispersion of AChN in PLA. However, with an increase in AChN loading level until up to 10 wt %, a strong diffraction peak located at 19.26° and a weak diffraction peak located at 9.14° appeared. The intensities of the diffraction peaks increased as the AChN loading level increased, which may be attributed to the presence of AChN as the crystalline filler phase. It also indicated the crystalline structure of the AChN was retained in the PLA/AChN nanocomposites.

Fractured Morphologies of PLA/AChN Nanocomposites

Figure 8 shows SEM images of the fracture morphologies of PLA/AChN nanocomposites as well as neat PLA film. The fractured surface of neat PLA film was smooth [Figure 8(A)]. When 1 wt % AChN was introduced into PLA, the fractured surface was straighter [Figure 8(B)], and when the loading levels were higher, such as 2 and 4 wt %, the straightened surfaces were more obvious and the original structure of the nanocomposites were maintained, as shown in Figure 8(C,D). With a continuous increase in the AChN loading level (6, 8, and 10 wt %), large conglomerations occurred in the nanocomposites, which indicated that the original structure of the PLA matrix were slightly damaged by the addition of AChN [shown in Figure 8(E–G)].

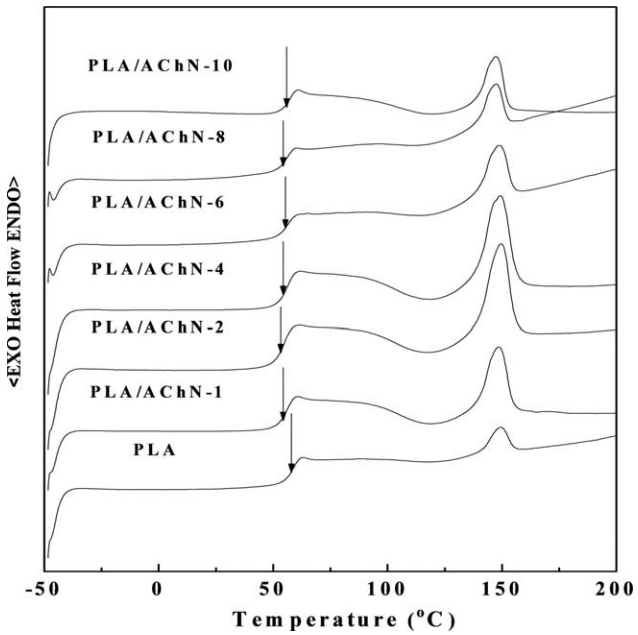

Figure 9. DSC thermograms of the PLA/AChN nanocomposite films containing various loading levels of AChN as well as the neat PLA film.

Table II. DSC Data of the PLA/AChN Nanocomposite Films as Well as Neat PLA Film

Sample no.	$T_{g,mid}$ (°C)	$\triangle C_P$ (J g^{-1} K^{-1})	$\triangle C_{P,PLA}$ (J g^{-1} K^{-1})	T_m (°C)	$\triangle H_m$ (J g^{-1})	$\triangle H_{m,PLA}$ (J g^{-1})	χ_c[a] (%)
PLA	57.7	0.54	0.54	149.6	4.9	4.9	5.3
PLA/AChN-1	54.7	0.41	0.41	148.6	12.2	12.3	13.2
PLA/AChN-2	53.7	0.42	0.43	149.6	11.5	11.7	12.6
PLA/AChN-4	55.0	0.36	0.38	149.3	12.7	13.2	14.2
PLA/AChN-6	55.7	0.45	0.48	148.6	11.3	12.0	12.9
PLA/AChN-8	55.4	0.60	0.66	147.6	8.8	9.6	10.3
PLA/AChN-10	55.8	0.39	0.43	147.2	9.6	11.2	12.0

[a] $\chi_c = \triangle H_m/\omega\triangle H_m^*$, where $\triangle H_m^*$ = 93.0 J g^{-1}, the heat of fusion 100% crystalline PLA[41], and ω is the weight fraction of the polymeric matrix material in the final product.

Thermal Properties of PLA/AChN Nanocomposites

DSC thermograms of the PLA/AChN nanocomposites and neat PLA films are depicted in Figure 9. The data for glass transition temperature at midpoint ($T_{g,\ mid}$) and heat-capacity increment (ΔC_p), as well as melting temperature (T_m) and heat enthalpy (ΔH_m) are summarized in Table II. The $T_{g,\ mid}$ and ΔC_p values of the PLA/AChN nanocomposites were both lower than those of the neat PLA film, which may be attributed to the AChN affecting interactions between the amorphous and crystalline domains, thus resulting in separation of the micro-phase between the amorphous and crystalline domains. The T_m values of all the PLA/AChN nanocomposites were lower than that of the neat PLA film, which may indicate that the size of the crystalline domain of the PLA matrix was changed by the compounds of PLA and AChN. The ΔH_m values of all the PLA/AChN nanocomposites were dramatically higher than that of the neat PLA film, which was attributed to the nucleation function of AChN for improving crystallinity of the PLA matrix.

Mechanical Properties of PLA/AChN Nanocomposites

Figure 10 shows the effects of AChN loading level on the mechanical properties of the PLA/AChN nanocomposites including tensile strength (σ_b), Young's modulus (E) and elongation at break (ε_b). The σ_b and E of the nanocomposites increased gradually with the increase in AChN loading level, until the AChN loading level was up to 4 wt %. σ_b and E reached the maximum values of 36.3 and 1573.8 MPa, respectively, which were in contrast to a tensile strength of 25.1 MPa and a Young's modulus of 1148.5 MPa for the neat PLA film, were increased by 45 and 37%, respectively. However, the ε_b of the nanocomposites gradually decreased with the increase in AChN loading level, and all were lower than that of the neat PLA film. When an appropriate amount of AChN (not higher than 4 wt %) was introduced into PLA, the acetylation of ChN promoted its dispersion in the PLA matrix and the strong interfacial adhesion between AChN and the PLA matrix contributed to the increase in σ_b and E, which was in consistent with SEM and DSC results. When excess AChN (6, 8, and 10 wt %) was introduced, the presence of rigid nanocrystals and a percolation network may have slightly damaged the original PLA structure, thus causing a decrease in σ_b and E, which were in consistent with SEM results. In this percolation mechanism, with regards to the nanocomposites filled with chitin nanocrystal, at high temperature, such as above T_g, the modulus of the filler is far higher than the matrix, which means that all the stiffness of the nanocomposites is due to infinite aggregates of the chitin nanocrystals. As a result, the parameter of φ, which is defined as the ratio of elastic shear modulus of the nanocomposite vs. the modulus of the filler, corresponds to the volume fraction of the percolating rigid phase, and it can be calculated by the following eq. (1):

$$\varphi = V_R\left(\frac{V_R - V_{Rc}}{1 - V_{Rc}}\right)^b \quad \text{for } V_R \geq V_{Rc} \tag{1}$$

where V_{Rc} is the critical volume fraction of the rigid phase at the percolation threshold and b is the corresponding critical exponent. The threshold fraction to reach the percolation of fillers strongly depends on the aspect ratio of the dispersed filler phase and on their orientation in space. For a random orientation, V_{Rc}, the volume fraction at the percolation threshold, depends on the aspect ratio (L/d) of the filler. In this case, the aspect ratio of AChN was about 14.5, leading to a V_{Rc} value of about 4.8 vol %, i.e., 7.2 wt %. The rigid

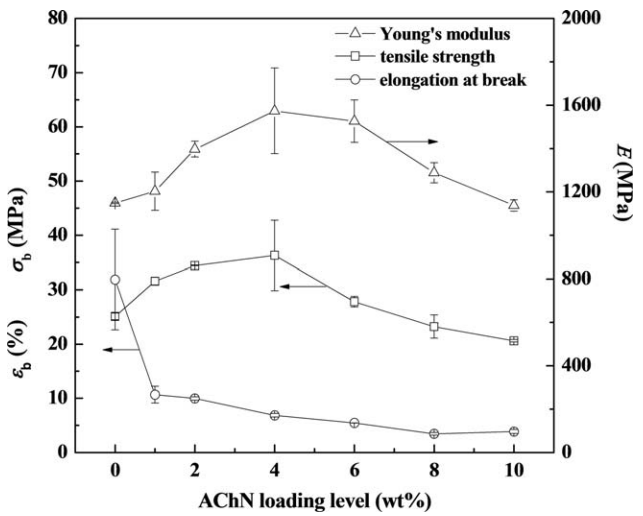

Figure 10. Effect of the AChNs loading level on tensile strength (σ_b), Young's modulus (E) and elongation at break (ε_b) for the PLA/AChN nanocomposite films and the neat PLA film.

AChN in the PLA matrix and the changes to original structure of the PLA matrix thereof, which was shown by the XRD and SEM results, caused a decrease in ε_b. The enhanced tensile strength and Young's modulus of the nanocomposites with the addition of AChN may contribute to increased applications for PLA in industry.

CONCLUSIONS

Chitin nanocrystals were surface acetylated by acetic anhydride, and the crystalline structure of ChN was maintained after the modification. The acetylated ChN was incorporated into a PLA matrix and when 4 wt % AChN was introduced, the tensile strength and Young's modulus of the PLA/AChN nanocomposites reached the maximum values, a 45 and 37% increase over the neat PLA film, respectively. This simultaneous enhancement could be attributed to the well dispersion of AChN in the PLA matrix and strong interfacial adhesion between AChN and PLA. However, the presence of rigid nanocrystals and the effects on the PLA matrix thereof caused a decreased elongation at break of the PLA/AChN nanocomposites. The good performance of this new nanocomposite material based on biodegradable PLA is believed to have good potential for the applications as the biomedical materials, such as scaffolds, bone-fixation devices and so on, and also as the thermoformed food/beverage serving utensils, such as plastic cups and plates, sanitary products, packaging containers and so on.

ACKNOWLEDGMENTS

The research work was financially supported by the Program of New Century Excellent Talents, Ministry of Education of China (NCET-11-0686); National Natural Science Foundation of China; Fundamental Research Funds for the Central Universities (Self-Determined and Innovative Research Funds of WUT 2012-Ia-006); ecoENERGY Innovation Initiative of Canada; Program of Energy Research and Development (PERD) of Canada and State Key Laboratory of Pulp and Paper Engineering, South China University of Technology (201212).

REFERENCES

1. Fortunati, E.; Armentano, I.; Zhou, Q.; Puglia, D.; Terenzi, A.; Berglund, L. A.; Kenny, J. M. *Polym. Degrad. Stab.* **2012**, *97*, 2027.
2. Bulota, M.; Kreitsmann, K.; Hughes, M.; Paltakari, J. *J. Appl. Polym. Sci.* **2012**, *126*, E449.
3. Frone, A. N.; Berlioz, S.; Chailan, J.-F.; Panaitescu, D. M.; Donescu, D. *Polym. Compos.* **2011**, *32*, 976.
4. Kose, R.; Kondo, T. *J. Appl. Polym. Sci.* **2013**, *128*, 1200.
5. Kim, H. K.; Kim, S. J.; Lee, H. S.; Choi, J. H.; Jeong, C. M.; Sung, M. H.; Park, S.-H.; Park, H. J. *J. Appl. Polym. Sci.* **2013**, *127*, 3823.
6. Kale, G.; Auras, R.; Singh, S. P. *J. Polym. Environ.* **2006**, *14*, 317.
7. Way, C.; Wu, D. Y.; Cram, D.; Dean, K.; Palombo, E. *J. Polym. Environ.* **2013**, *21*, 54.
8. Schwach, E.; Six, J. L.; Avérous L. *J. Polym. Environ.* **2008**, *16*, 286.
9. Pinto, A. M.; Moreira, S.; Goçalves, I. C.; Gama, F. M.; Mendes, A. M.; Magalhães, F. D. *Colloid Surface B.* **2013**, *104*, 229.
10. Quero, F.; Eichhorn, S. J.; Nogi, M.; Yano, H.; Lee, K.-Y.; Bismarck, A. *J. Polym. Environ.* **2012**, *20*, 916.
11. Martínez-Sanz, M.; Lopez-Rubio, A.; Lagaron, J. M. *Biomacromolecules* **2012**, *13*, 3887.
12. Habibi, Y.; Lucia, L. A.; Rojas, O. J. *Chem. Rev.* **2010**, *110*, 3479.
13. Lin, N.; Chen, G.; Huang, J.; Dufresne, A.; Chang, P. R. *J. Appl. Polym. Sci.* **2009**, *113*, 3417.
14. Zhang, X.; Huang, J.; Chang, P. R.; Li, J.; Chen, Y.; Wang, D.; Yu, J.; Chen, J. *Polymer* **2010**, *51*, 4398.
15. Sanchez-Garcia, M.; Lagaron, J. *Cellulose.* **2010**, *17*, 987.
16. Okubo, K.; Fujii, T.; Thostenson, E. T. *Compos. A Appl. S.* **2009**, *40*, 469.
17. Fox, D. M.; Lee, J.; Citro, C. J.; Novy, M. *Polym. Degrad. Stab.* **2013**, *98*, 590.
18. Frone, A. N.; Berlioz, S.; Chailan, J.-F.; Panaitescu, D. M. *Carbohydr. Polym.* **2013**, *91*, 377.
19. Ifuku, S.; Nogi, M.; Abe, K.; Handa, K.; Nakatsubo, F.; Yano, H. *Biomacromolecules* **2007**, *8*, 1973.
20. Gattin, R.; Copinet, A.; Bertrand, C.; Couturier, Y. *Int. Biodeterior. Biodegrad.* **2002**, *50*, 25.
21. Xue, P.; Wang, K.; Jia, M.; Yang, M. *J. Wuhan Univ. Technol. Mater. Sci. Ed.* **2013**, *28*, 157.
22. Phetwarotai, W.; Potiyaraj, P.; Aht-Ong, D. *J. Appl. Polym. Sci.* **2012**, *126*, E162.
23. Martin, O.; Avérous, L. *Polymer* **2001**, *42*, 6209.
24. Le Bolay, N.; Lamure, A.; Leis, N. G.; Subhani, A. *Chem. Eng. Process.* **2012**, *56*, 1.
25. Azizi Samir, M. A. S.; Alloin, F.; Dufresne, A. *Biomacromolecules* **2005**, *6*, 612.
26. Azizi Samir, M. A. S.; Chazeau, L.; Alloin, F.; Cavaillé, J.-Y.; Dufresne, A.; Sanchez, J.-Y. *Electrochim. Acta.* **2005**, *50*, 3897.
27. Lin, N.; Huang, J.; Chang, P. R.; Feng, J.; Yu, J. *Carbohydr. Polym.* **2011**, *83*, 1834.
28. Jonoobi, M.; Mathew, A. P.; Abdi, M. M.; Makinejad, M. D.; Oksman, K. *J. Polym. Environ.* **2012**, *20*, 991.
29. Tome, L. C.; Pinto, R. J. B.; Trovatti, E.; Freire, C. S. R.; Silvestre, A. J. D.; Neto, C. P.; Gandini, A. *Green Chem.* **2011**, *13*, 419.
30. Mine, S.; Izawa, H.; Kaneko, Y.; Kadokawa, J.-I. *Carbohydr. Res.* **2009**, *344*, 2263.
31. Muzzarelli, R. A. A. Chitin; Pergamon Press: Oxford, **1977**; p 220.
32. Muzzarelli, R. A. A.; Jeuniaux, C.; Gooday, G. W. Chitin in Nature and Technology; Plenum Press: New York, **1986**; p 254.
33. Zeng, J. B.; He, Y. S.; Li, S. L.; Wang, Y. H. *Biomacromolecules.* **2012**, *13*, 1.

34. Nair, K. G.; Dufresne, A. *Biomacromolecules.* **2003**, *4*, 657.

35. Minke, R.; Blackwell, J. *J. Mol. Biol.* **1978**, *120*, 167.

36. Uddin, A. J.; Fujie, M.; Sembo, S.; Gotoh, Y. *Carbohydr. Polym.* **2012**, *87*, 799.

37. Ji, Y.-L.; Wolfe, P. S.; Rodriguez, I. A.; Bowlin, G. L. *Carbohydr. Polym.* **2012**, *87*, 2313.

38. Kadokawa, J.-I.; Takegawa, A.; Mine, S.; Prasad, K. *Carbohydr. Polym.* **2011**, *84*, 1408.

39. Chang, P. R.; Jian, R. J.; Yu, J. G.; Ma, X. F. *Carbohydr. Polym.* **2010**, *80*, 420.

40. Huang, J.; Zou, J. W.; Chang, P. R.; Yu, J. H.; Dufresne, A. *eXPRESS Polym. Lett.* **2011**, *5*, 362.

41. Martin, O.; Averous, L. *Polymer* **2001**, *42*, 6209.